JOURNAL OF GUIDANCE, CONTROL, AND DYNAMICS
Vol. 28, No. 3, May–June 2005

Suppression of Control Reversal Using Leading- and Trailing-Edge Control Surfaces

George Platanitis* and Thomas W. Strganac†
Texas A&M University, College Station, Texas 77843-3141

Control reversal is the loss, due to the flexibility of the primary aerostructure, of aircraft maneuvering loads induced by control surfaces. In recent years, attention has been given to the suppression of reversal through the use of distributed control surfaces. The authors study reversal behavior for a wing section with full-span leading-edge and trailing-edge control surfaces. The essential equations are developed by examining static aeroelastic responses. Analysis and experiments are presented. Specific trailing-edge to leading-edge control commands are identified to optimize performance. Although reversal is not eliminated in the experiments, the addition of the leading edge is shown to improve performance substantially. The research also identifies the adverse consequences of actuator flexibility.

Nomenclature

C_l	=	wing section lift coefficient
$C_{l\alpha}$	=	$\partial C_l/\partial\alpha$
$C_{l\beta}$	=	$\partial C_l/\partial\beta$
$C_{l\gamma}$	=	$\partial C_l/\partial\gamma$
$C_{m\text{-}c/4}$	=	wing section moment coefficient at quarter-chord
$C_{m\alpha}$	=	$\partial C_{m\text{-}c/4}/\partial\alpha$
$C_{m\beta}$	=	$\partial C_{m\text{-}c/4}/\partial\beta$
$C_{m\gamma}$	=	$\partial C_{m\text{-}c/4}/\partial\gamma$
c	=	chord length
e	=	distance from elastic axis to aerodynamic center
f_{le}	=	length of leading edge control surface in fraction of chord
f_{te}	=	length of trailing edge control surface in fraction of chord
h	=	plunge displacement
k_h	=	plunge stiffness
k_a	=	pitch stiffness
q	=	dynamic pressure
r	=	gearing ratio, γ/β
S	=	wing section surface area
α	=	pitch rotation, angle of attack measured from zero-lift line
β	=	trailing edge control surface deflection
γ	=	leading edge control surface deflection
λ	=	nondimensional dynamic pressure $= qSc/k_a$
ρ	=	air density

Introduction

ONE particular area in the field of aeroelasticity for which the theory is well developed, yet benchmark experiments with multiple actuated surfaces are limited, is control reversal.[1] For example, roll reversal occurs for an aircraft when the aircraft loses roll control effectiveness due to the flexibility of the wing structure to which a control surface is attached. In such a case, a wing with the typical trailing-edge control surface (TECS) will undergo a twist response due to a control input in addition to twist due to other aeroelastic load effects. Reversal occurs when the twist due to the control-surface deflection negates the control-induced maneuvering loads. Essentially, although the control surface generates additional lift for the maneuver, the twist response due to the control input untwists the wing and thereby reduces the effective angle of attack. At the onset of reversal, the net effect is zero lift and, as a consequence, no maneuver loads. This response depends upon flight conditions such as dynamic pressure and Mach number. Beyond the flight conditions for the onset of reversal, roll-control effectiveness is negative, where the aircraft roll response occurs in the opposite direction. The behavior occurs in large transport aircraft, high-performance fighters, and sailplanes. Design features such as wing sweep and the use of in-board ailerons will raise the flight conditions at which reversal occurs. Nonetheless, reversal limits performance.

In one study,[2] reversal trends were examined in the transonic region using numerical computations of the flowfield. The impact of the interaction between control-surface actuation, structural flexibility, and nonlinear aerodynamics (including the presence of shock waves) was investigated using a nonlinear flow solver, with results compared to conventional, linear predictions. The presence of shocks caused an increase in adverse twist, degrading control-surface effectiveness further than predicted by linear theory. Other studies of reversal behavior, including the use of active control methods to improve effectiveness of a TECS by using a leading-edge control surface (LECS), have been pursued through programs such as the Active Flexible Wing program,[3] now known as the Active Aeroelastic Wing program.[4] These investigations also involved wind-tunnel experiments using a wing configuration for a fighter aircraft. Yet ground-based experiments on the aeroelastic system with multiple control surfaces including LECS devices and, in particular, how such a design impacts the performance of a multicontrol configuration, are limited.

Woods-Vedeler et al.[3] developed control laws to minimize roll maneuver loads. Traditionally, design engineers added structure to wings to increase stiffness to avoid roll reversal (and other unfavorable aeroelastic responses) of aircraft in the flight envelope. Without active control, these passive means were necessary to alleviate unfavorable responses. This design practice required optimizing stiffness with weight penalties, and flexibility effects were not directly accounted for in the wing performance. The Woods-Vedeler studies found it possible to use the inboard TECS to maintain desired roll performance by using both the outboard leading- and trailing-edge control surfaces to minimize wing twist. The control laws developed for this configuration were tested below and above the open-loop flutter dynamic pressure. In their studies a flutter suppression system was used as well. Torsion moment loads were reduced, whereas bending moment reductions showed mixed results. The control laws

Presented as Paper 2003-1488 at the AIAA 44th Structures, Structural Dynamics, and Materials Conference, Norfolk, VA, 21–25 April 2003; received 24 November 2003; revision received 9 January 2004; accepted for publication 13 January 2004.

*Graduate Research Assistant, Department of Aerospace Engineering.
†Associate Professor, Department of Aerospace Engineering, 3141 TAMU. Associate Fellow AIAA.

were shown to effectively reduce incremental torsion loads on the AFW wind-tunnel model.

Andersen et al.[4] studied the effectiveness of using multiple control surfaces to achieve a desired roll trim of a fighter aircraft. The use of active control, especially with multiple control surfaces, on a more flexible wing allowed efficient use of maneuver-control power, minimal structural loads, and drag reduction. The use of a LECS provides additional control authority, as it complements the TECS to improve aircraft wing performance. Andersen et al. noted that the effectiveness of the TECS was always lost at a critical dynamic pressure (onset of reversal), whereas the LECS maintained roll effectiveness for higher dynamic pressures. Thus, the potential for using an LECS to counter reversal effects was realized. Structural deformations were calculated by the finite element method, whereas a linear panel method was used to simulate aerodynamic loads. Roll trim was investigated over a range of dynamic pressures for various multiple-control-surface configurations and for reduced wing stiffness. A reduction in the structural stiffness did not change the required control effort very much for a desired roll rate, suggesting that weight savings may be realized by lowering the wing stiffness, because a lower stiffness suggests a lower structural mass.

Here, reversal behavior and lift effectiveness is examined using a typical two-degree-of-freedom section model and validated through wind-tunnel experiments that use a wing section with leading- and trailing-edge control surfaces. It will be shown that with appropriate selections of control-surface deflection ratios, reversal effects may be delayed. The effects of actuator stiffness effects and the consequences of aerodynamic nonlinearities will also be considered.

Static Aeroelastic Behavior

In this section, the equations for reversal, divergence, and lift effectiveness for the wing section with leading- and trailing-edge control surfaces are developed. Although the development of the aeroelastic equations for the typical section is found in several texts, here we add a leading-edge control surface and adopt an approach similar to that of Dowell et al.[5]

If one considers twist about the elastic axis of a rigid wing section mounted on an elastic support as depicted in Fig. 1, the following torsion and translation equations for equilibrium hold:

$$L - k_h h = 0 \tag{1a}$$

$$M - k_\alpha \alpha = 0 \tag{1b}$$

The static aerodynamic lift and moment L and M, with the moment taken about the elastic axis, of the wing section are given by

$$L = qSC_{l\alpha}\alpha + qSC_{l\beta}\beta + qSC_{l\gamma}\gamma \tag{2a}$$

$$M = Le + M_{c/4} = Le + qScC_{m\alpha}\alpha + qScC_{m\beta}\beta + qScC_{m\gamma}\gamma \tag{2b}$$

where α is measured from the zero-lift line and the moment coefficients are referenced to the quarter-chord. Flow separation is ignored; thus, the aerodynamic derivatives are assumed to be constant. The wing section being used here is symmetric; thus $C_{m\alpha} = 0$. Although the equations do not reflect the possibility of aerodynamic loads at zero angle of attack, it is recognized that, in general, such loads may exist, but a primary objective here is to examine the change in maneuver loads due to a control input. Initially, the flexibility of the control surface actuators is assumed to be negligible, but this assumption will be tested herein.

We observe that aerodynamic loads leading to a maneuver, such as a roll, will only occur if a lift force is generated. It is noted that control inputs lead to changes in both aerodynamic lift and moment loads, and the moment may lead to a wing twist response that decreases the angle of attack. As a consequence, reversal occurs when the additional lift L generated by a control input is zero ($L = 0$) regardless of the TECS control input. A primary purpose of the LECS is to prevent the wing twist response from the TECS that tends to decreases the angle of attack.

By substituting Eq. (2a) into Eq. (2b) and substituting this equation into Eq. (1b), an equation for pitch response due to control inputs is found:

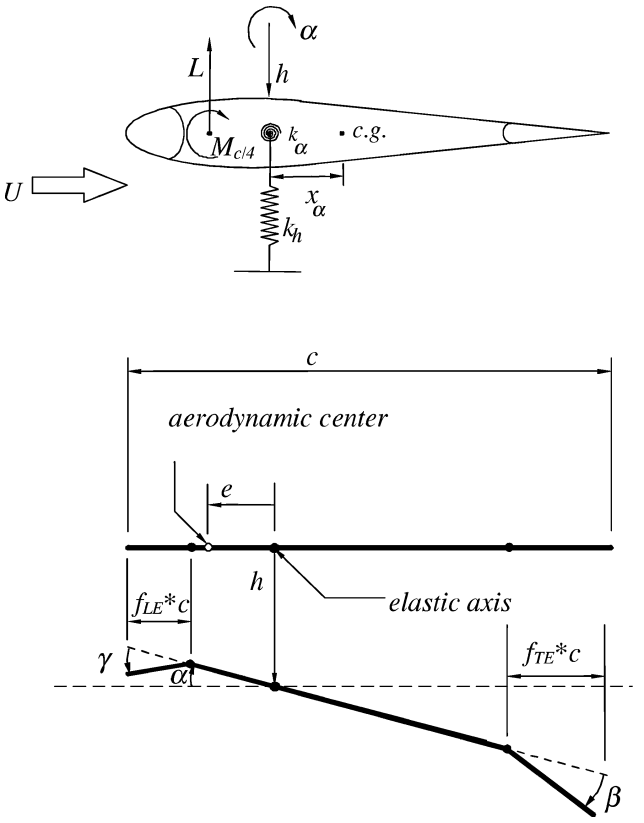

Fig. 1 Geometry of the wing section shown with leading- and trailing-edge control surfaces.

$$\alpha = \frac{(qSC_{l\beta}e + qScC_{m\beta})\beta}{k_\alpha - qSC_{l\alpha}e} + \frac{(qSC_{l\gamma}e + qScC_{m\gamma})\gamma}{k_\alpha - qSC_{l\alpha}e} \tag{3}$$

Equation (3) is derived from moment equilibrium and indicates that the angle of attack of the wing is affected by the control input. To find an expression for the reversal conditions, Eq. (3) is substituted into the lift expression, Eq. (2a), which leads to an equation for the lift due directly to control inputs. Then, by examining the condition at reversal ($L = 0$) and solving for the associated dynamic pressure, the equation for the reversal dynamic pressure in terms of the control input is found:

$$q_{\text{REV}} = -\frac{k_\alpha(C_{l\beta}\beta + C_{l\gamma}\gamma)}{SC_{l\alpha}c(C_{m\beta}\beta + C_{m\gamma}\gamma)} \tag{4}$$

Thus, a dynamic pressure, q_{REV}, at which reversal occurs is equivalent to a specific set of physical parameters. For example, as one might expect, the conditions for reversal improve for a wing with greater stiffness. Note that, if one eliminates the effect of the LECS (set $\gamma = 0$), then the more familiar equation for reversal is obtained for a wing section with a TECS only. At reversal, no lift is generated (thus, no maneuver load) regardless of the TECS deflection.

A deflection ratio r is defined such that $r = \gamma/\beta$. This ratio is also referred to as the "gearing ratio" because a selected value of r dictates the deflection of the LECS control surface given a specific input to the TECS. Thus, Eq. (4) may be written as

$$q_{\text{REV}} = -\frac{k_\alpha(C_{l\beta} + rC_{l\gamma})}{SC_{l\alpha}c(C_{m\beta} + rC_{m\gamma})} \tag{5}$$

From Eq. (5), it can be seen from the denominator that $q_{\text{REV}} \to \infty$ when $r = -C_{m\beta}/C_{m\gamma}$. Therefore, at this value of the gearing ratio and beyond, reversal does not occur regardless of dynamic pressure. This will be further clarified upon examination of results. It is noted that the gearing ratio does not address the impact of the magnitude

of the control input, and responses at gearing ratios from larger deflections will be adversely affected by flow separation.

Equation (5) may be written in an alternate form by defining a nondimensional dynamic pressure as

$$\lambda = qSc/k_\alpha \tag{6}$$

Thus, in coefficient form, the conditions for reversal may be expressed as

$$\lambda_{\text{REV}} = -\frac{(C_{l\beta} + rC_{l\gamma})}{C_{l\alpha}(C_{m\beta} + rC_{m\gamma})} \tag{7}$$

The presence of aeroelastic divergence affects the characteristics of reversal. Aeroelastic divergence is a static instability in which the deformation-dependent aerodynamic loads exceed the stiffness-dependent structural restoring loads. Using Eq. (3), the divergence pressure, q_{DIV}, is found when one considers that $\alpha \to \infty$ (and $L \to \infty$) at divergence. Singularities appear in the terms of Eq. (3), and by setting the denominator of the terms in Eq. (3) to zero, the divergence pressure is found as

$$q_{\text{DIV}} = k_\alpha / SeC_{l\alpha} \tag{8}$$

or, in dimensionless form,

$$\lambda_{\text{DIV}} = (1/C_{l\alpha})(c/e) \tag{9}$$

Note that $\lambda_{\text{DIV}} \to \infty$ when $e = 0$ (the elastic axis coincides with the aerodynamic center). Also, as suggested by either Eq. (8) or Eq. (9), divergence is not physically possible if $e < 0$. Substituting Eq. (9) and $\gamma = r\beta$ into Eq. (3) gives

$$\alpha = [\lambda/(1 - \lambda/\lambda_{\text{DIV}})][(C_{l\beta} + rC_{l\gamma})(e/c) + (C_{m\beta} + rC_{m\gamma})]\beta \tag{10}$$

which is an equation for pitch response in terms of the TECS deflection at a specific gearing ratio. Expressing the equation for lift, Eq. (1a), in coefficient form and using $\gamma = r\beta$ gives

$$C_L = C_{l\alpha}\alpha + (C_{l\beta} + rC_{l\gamma})\beta \tag{11}$$

Substituting Eq. (10) into (11) yields

$$C_L = \left\{ \frac{\lambda C_{l\alpha}}{1 - \lambda/\lambda_{\text{DIV}}} \left[(C_{l\beta} + rC_{l\gamma})\frac{e}{c} + (C_{m\beta} + rC_{m\gamma}) \right] + (C_{l\beta} + rC_{l\gamma}) \right\} \beta \tag{12}$$

Equation (7) is solved for $(C_{m\beta} + rC_{m\gamma})$ and substituted into Eq. (12), resulting in the common factor $(C_{l\beta} + rC_{l\gamma})$. Dividing Eq. (12) through by $(C_{l\beta} + rC_{l\gamma})\beta$ gives

$$\frac{C_L}{(C_{l\beta} + rC_{l\gamma})\beta} = \frac{\lambda C_{l\alpha}}{1 - \lambda/\lambda_{\text{DIV}}} \left[\frac{e}{c} - \frac{1}{C_{l\alpha}\lambda_{\text{REV}}} \right] + 1 \tag{13}$$

This equation may be rewritten for lift effectiveness. Consider

$$C_L/(C_{l\beta} + rC_{l\gamma})\beta = [\lambda/(1 - \lambda/\lambda_{\text{DIV}})][C_{l\alpha}(e/c) - 1/\lambda_{\text{REV}}] + 1$$
$$= [\lambda/(1 - \lambda/\lambda_{\text{DIV}})][1/\lambda_{\text{DIV}} - 1/\lambda_{\text{REV}}] + 1 \tag{14}$$

which may be rearranged as

$$\frac{L_{\text{flex}}}{L_{\text{rigid}}} \equiv L_{\text{eff}} = \frac{C_L}{(C_{l\beta} + rC_{l\gamma})\beta} = \frac{1 - \lambda/\lambda_{\text{REV}}}{1 - \lambda/\lambda_{\text{DIV}}} \tag{15}$$

where $L_{\text{flex}}/L_{\text{rigid}}$ is the ratio of the lift generated by the flexible wing to the lift of the rigid wing and defined as lift effectiveness L_{eff}, which is a measure of roll performance (reversal occurs when this ratio is zero). Note that, if $r = 0$, then the result for a wing section with a TECS only is obtained, which is

$$L_{\text{eff}} = \frac{C_L}{C_{l\beta}\beta} = \frac{1 - \lambda/\lambda_{\text{REV}}}{1 - \lambda/\lambda_{\text{DIV}}} \tag{16}$$

We note that reversal occurs as $\lambda \Rightarrow \lambda_{\text{REV}}$ and divergence occurs as $\lambda \Rightarrow \lambda_{\text{DIV}}$, and the physical parameters of the system dictate which aeroelastic anomaly, λ_{DIV} or λ_{REV}, occurs at the lower dynamic pressure. Also, we note that λ_{DIV} depends on the aerodynamic eccentricity e, the value of which may be positive, negative, or zero and will dictate whether lift effectiveness increases or decreases as dynamic pressure increases. If the wing section does not have any control surfaces, then reversal disappears and the preceding equation reduces to

$$L_{\text{eff}} = 1/(1 - \lambda/\lambda_{\text{DIV}}) = 1/(1 - \lambda C_{l\alpha}e/c) \tag{17}$$

which indicates that lift effectiveness approaches infinity as divergence is approached (for $e > 0$).

Lift L is directly measured in our wind-tunnel experiments. Thus, Eq. (15) is slightly modified to

$$L_{\text{eff}} = \frac{C_L}{(C_{l\beta} + rC_{l\gamma})\beta} = \frac{L/qS}{(C_{l\beta} + rC_{l\gamma})\beta} \tag{18}$$

Some limiting responses of interest are revealed when one examines select values of the gearing ratio r. For example, from Eq. (5), it was noted that $q_{\text{REV}} \to \infty$ when $r = -C_{m\beta}/C_{m\gamma}$. For this value of $r = r_{q_{\text{REV}} \to \infty}$, control performance (as measured by lift effectiveness) will deteriorate for increasing values of q but reversal will not occur. Another value of particular interest is $r_{L_{\text{eff}}=1}$, where lift effectiveness remains unchanged regardless of control input. In effect, $r_{L_{\text{eff}}=1}$ represents an equivalent infinitely stiff system (i.e., a rigid wing) and lift generated by the control input increases linearly with q. Using Eq. (15) and setting $L_{\text{eff}} = 1$ yields

$$[\lambda_{\text{REV}} = \lambda_{\text{DIV}}]_{L_{\text{eff}}=1} \tag{19}$$

which is representative of considering a rigid wing; that is, both the reversal and divergence conditions become very large as the wing becomes very stiff.

Using the definition of λ_{REV} in Eq. (7), the definition of λ_{DIV} in Eq. (9), and the realization that $\lambda_{\text{DIV}} = \lambda_{\text{REV}}$ at $L_{\text{eff}} = 1$ yield

$$\frac{-(C_{l\beta} + rC_{l\gamma})}{C_{l\alpha}(C_{m\beta} + rC_{m\beta})} = \frac{1}{C_{l\alpha}}\frac{c}{e} \tag{20}$$

Rearranging Eq. (20) for r (at $L_{\text{eff}} = 1$) gives

$$r_{L_{\text{eff}}=1} = \frac{-[C_{l\beta} + (c/e)C_{m\beta}]}{[C_{l\gamma} + (c/e)C_{m\gamma}]} \tag{21}$$

which represents the case of an ideal rigid wing that is free of reversal (and divergence).

Experiment Hardware

For this investigation, a new wing section with a leading- and trailing-edge control surface has been built for experiments on the Nonlinear Aeroelastic Test Apparatus (NATA) in the Texas A&M University 2 Ft × 3 Ft Low Speed Wind Tunnel. As described in Refs. 6–11, NATA has been used in several studies of free and controlled dynamic aeroelastic response. A unique feature of NATA is the presence of two cams that are fabricated to permit both prescribed linear and nonlinear responses in pitch and plunge, depending on the experimental requirements. For the research presented here, the linear configuration is used.

Key parameters of the experiment are given in Table 1. The elastic axis position e may be changed easily by attaching the wing model to one of several attachment stations on NATA. In the investigations, three different stations are used and will be further discussed under Results. Also, frictional forces will affect proper interpretation of

measurements intended to determine static response; consequently, viscous (c) and Coulomb (μ) damping parameters are indicated in Table 1. Additional NATA information is reported by O'Neil[7] and Block.[8]

Figure 1 defines the wing-section geometry. Figure 2 shows photographs of the planform and edge views of the wing-section. The wing-section profile approximates that of a NACA 0012 airfoil with a maximum thickness of 12% chord. The length of the leading- and trailing-edge control surfaces are $f_{\mathrm{LE}} = 0.15$ and $f_{\mathrm{TE}} = 0.20$% chord lengths, respectively, with f representing the chord length fractions depicted in Fig. 1. Two E2-1024-375-H optical encoders are mounted on the rotation shafts of the leading- and trailing-edge control surfaces to measure control-surface deflections for comparison to the commanded inputs. A US Digital ED2 display box provides real-time indication of encoder output. Two FUTABA S9402 servomotors actuate the control surfaces, each motor being capable of generating 0.654 N-m of torque at 5 V, with deflections of the control surfaces linearly proportional to the applied voltage. A custom module in the acquisition software developed in LabVIEW® is used both to actuate the control surfaces by step inputs and to read their displacements. Incrementally, the control surfaces can be deflected to accurate test positions, thus overcoming actuator flexibility problems. Additional information for the new wing-section setup may be found in Platanitis and Strganac.[12]

Table 1 System parameters

Parameter	Value
c	0.3810 m
s	0.5945 m
k_h	2844 N/m
k_α	7.445 N m/rad
c_h	27.43 kg/s
c_α	0.03600 kg m^2/s
f_{LE}	0.15
f_{TE}	0.20
μ_h	0.02524
μ_α	0.01253

The static pitch and plunge responses of the wing section are measured for a given input to each of the control-surfaces. A control surface deflection leads to a change in the angle of attack, which produces a lifting force. This increased lift is due to the change in angle of attack of the wing due to pitch rotation about the elastic axis as well as the direct contribution of the deflected control surface. This lift force is determined using the measured displacement of the plunge carriage [see Eq. (1a)].

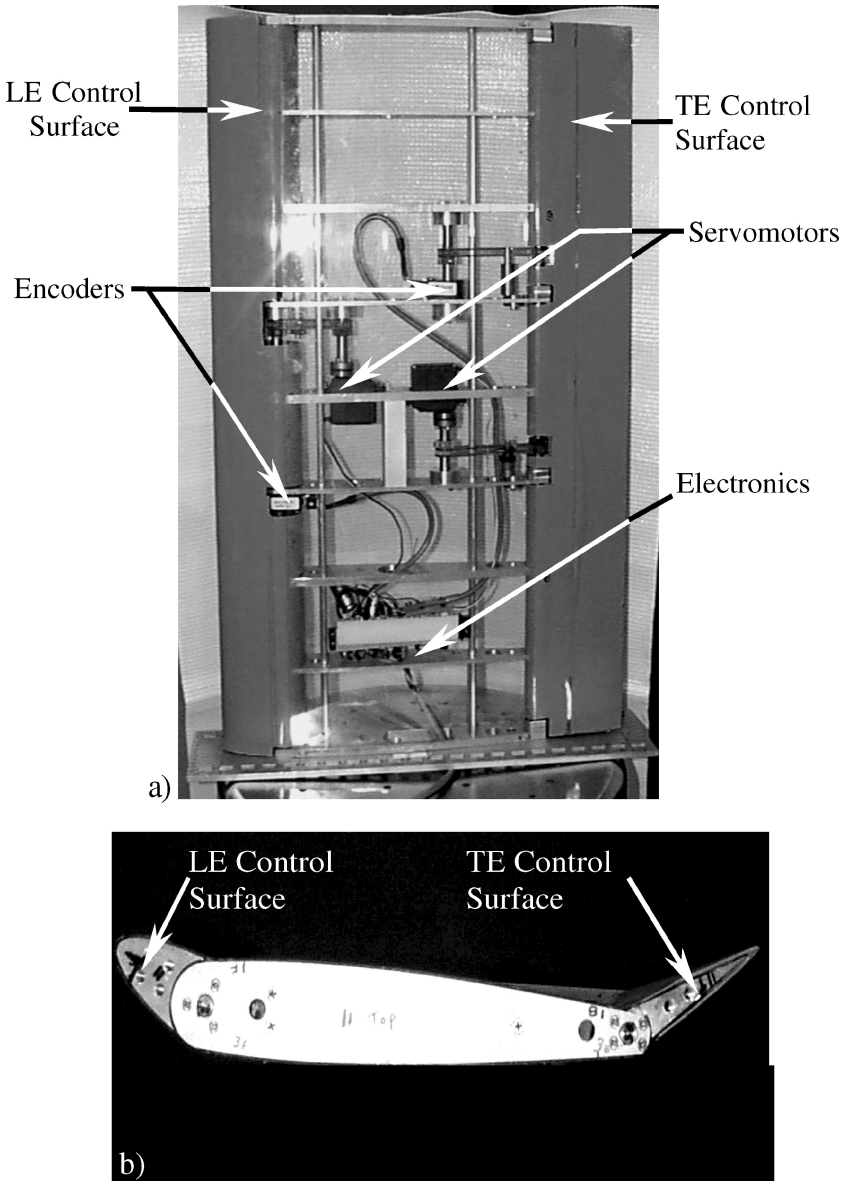

Fig. 2 Two-control-surface wing section: a) planform view with transparent skin-surface-revealing actuators, encoders, connections, and mechanical design and b) edge view with control surfaces deflected.

The following approach is used to investigate the lift effectiveness for several gearing ratios of control-surface deflection. The approach is duplicated for each elastic-axis location. First, for a given gearing ratio, the lift produced is measured directly for several freestream velocities. The desired control-surface deflections are approached in small increments during the experiment to minimize any initial oscillations resulting from step commands, thus facilitating more rapid measurement of static displacements. Because of actuator flexibility, both β and γ are measured and adjusted incrementally to ensure that the actual test values of β and γ are achieved. Then, noting the freestream velocity, control-surface deflection ratio, and TECS input, Eq. (18) is applied with the values of $C_{l\beta}$ and $C_{l\gamma}$ (found by a computational method described in the next section) to determine lift effectiveness. Measured and computed values of the lift effectiveness may be compared.

To validate the aerodynamic derivatives found by computational methods, additional experiments are performed. By placing the elastic axis to coincide with the quarter-chord (which is also the aerodynamic center) and individually locking one of the two degrees of freedom, lift and moment responses are directly measured for each of the angle-of-attack settings and control-surface deflections. With the control-surface positions fixed at zero deflection, the lift at fixed angles of attack may be measured. With the angle of attack fixed to zero and each control surface considered separately, the lift at fixed control-surface deflections may be measured. Finally, with the plunge degree of freedom fixed, the moments produced by individual control-surface deflections may be determined from the pitch response. It is necessary to perform these experiments at sufficient freestream velocities (10 m/s or greater) to generate aerodynamic loads adequate to overcome measurement errors at very low velocities.

Results

Table 2 compares the aerodynamic derivatives found by a computational model to those measured by experiments described in the previous section. The computational approach is a panel method (Smith-Hess) based on the approach described by Anderson.[13]

Table 2 Aerodynamic derivative coefficients

Variable	Numerical	Experimental	Std. error	R^2
$C_{l\alpha}$	6.757	6.441	0.03290	0.9838
$C_{l\beta}$	3.774	3.051	0.02017	0.9788
$C_{m\beta}$	−0.6719	−0.5133	0.004749	0.9770
$C_{l\gamma}$	−0.1566	−0.1717	0.002824	0.9548
$C_{m\gamma}$	−0.1005	−0.1126	0.002202	0.8979

The experimentally derived aerodynamic derivative values in Table 2 are found by performing a least-squares fit[14] for the data points in the linear region of the aerodynamic measurements. From measured lift and moment data, the load coefficients, C_L and C_M, are defined using Eqs. (1) and (2) as follows:

$$L = k_h h = qSC_L, \qquad L/qS = C_L$$
$$M_{c/4} = k_\alpha \alpha = qScC_M, \qquad M_{c/4}/qSc = C_M \tag{22}$$

where C_L is the lift coefficient and C_M is the moment coefficient about the quarter-chord. For these experiments, the elastic axis is set to coincide with the quarter-chord. The contributions of α, β, and γ are found from individual measurements. The aerodynamic derivatives are found from the slope of the lift (or moment) vs angle curves, with the angle being α, β, or γ depending on the derivative of interest.

The experimental values are consistent with theory, and the theoretical values are used in subsequent analysis because they have been validated by experiments. Some slight discrepancies between the theoretical and measured values are noted. A measure of the data fit is given by the R^2 values and the uncertainty in the data is indicated by the standard error (variance). Overall, the data fits appear good, although a little less so for $C_{m\gamma}$, as only a limited number of quality data could be obtained for this measurement due to the low moment loads for this geometry. A potential source of error is the binding forces due to frictional sources within the mechanical system. This error is minimized by repeating measurements, in addition to deliberately disturbing the system from equilibrium and confirming that the system restores itself to the original equilibrium position (i.e., we pluck the system). Also, flow separation at large angles of attack or large deflection angles will be present. This will be particularly true for the LECS data. Thus, it is necessary to test under conditions that provide forces sufficient for satisfactory measurable deflections, yet at angles sufficiently small to minimize flow separation.

Two forms of adverse aeroelastic behavior may be present in the experiments: reversal, at which maneuver loads are lost, and divergence, at which aeroelastic structural stability is lost. Here, gearing ratios r are examined to improve the conditions for reversal. For practical considerations (i.e., safety in experiments), it is desired to have $\lambda_{\mathrm{DIV}} > \lambda_{\mathrm{REV}}$. Yet we are interested in the case where $\lambda_{\mathrm{REV}} \to \infty$ when $r = -C_{m\beta}/C_{m\gamma}$ $(= r_{q_{\mathrm{REV}} \to \infty})$, which suggests for particular designs (i.e., elastic axis positions) that divergence will be the limiting condition. Such cases are examined with awareness of safety issues.

A method for demonstrating reversal is to examine lift per unit control input, which can be considered a measure of control (e.g., roll) power. Figure 3 shows L_β (lift per degree of TECS

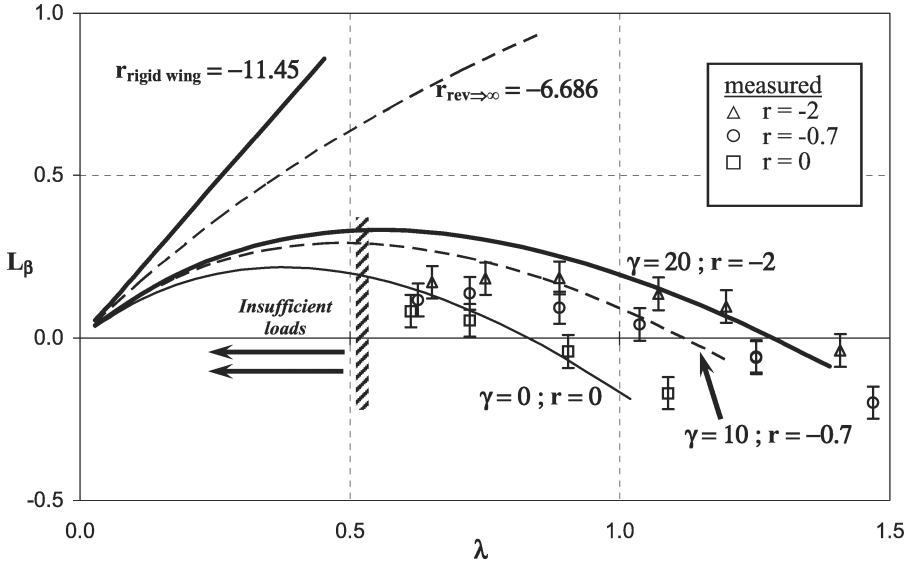

Fig. 3 Lift per TECS (β) deflection for the $e/c = -0.08595$ configuration. Error bars reflect a measurement uncertainty in L_β of ± 0.05 N/deg.

deflection) for increasing dynamic pressure. In this configuration, $e/c = -0.08595$. To generate the family of curves shown, the LECS deflection is set and the lift due to the TECS deflection over a range of freestream velocities is measured. We note that the sign of each individual control-surface deflection is required in full analysis since, for example, $\gamma/\beta = -10/5$ will cause a maneuver opposite to $\gamma/\beta = 10/-5$ even though $r = -2$ for both cases. In our experiments, we measure displacement of a wing section with a symmetric airfoil. The magnitude of the generated lift is the same for a given r, but the direction of displacement depends on the sign of the TECS. Again, it is noted that unmodeled flow separation will occur at large angles, especially for the LECS.

Reversal occurs when $L_\beta = 0$, and Fig. 3 clearly illustrates how reversal is delayed by a judicious choice of gearing ratio. Several gearing-ratio settings are examined, including $r = 0$, representing the baseline case where the leading edge is not active, $r = r_{q_{\mathrm{REV}} \to \infty} = -6.686$, representing the case in which reversal is eliminated completely, and $r = r_{L_{\mathrm{eff}}=1} = -11.45$, representing the limiting case of a rigid wing. For the latter case, although the lift effectiveness remains unchanged regardless of dynamic pressure, control power (L_β) grows in a linear manner with respect to dynamic pressure, thereby providing optimum performance.

As one can observe in Fig. 3, control performance for a particular setting is initially characterized by an increase in L_β as dynamic pressure increases. Yet, because of flexibility effects of the primary structure, a maximum value is achieved, after which control power deteriorates through reversal at $L_\beta = 0$. It is noted that experimental data could not be satisfactorily measured at low dynamic pressures, as indicated in the figure, because the loads were insufficient to overcome friction forces adequately. Although performance is improved by appropriate choices of gearing ratio, the best case representing the rigid-wing scenario is not achieved in the experiments. This is primarily due to nonlinearities such as flow separation that are present in the aerodynamic loads, as well as actuator flexibilities that exist in the physical system.

Following the approach described in Ref. 14, error bars are shown with the data points and reflect uncertainty in the measured L_β of ± 0.05 N/deg TECS deflection. This is equivalent to approximately 0.0003 m of plunge displacement, accounting for the encoder resolution and measurement errors caused by frictional forces. These uncertainties are representative of the level in all results presented here. Although comparisons may be viewed as unsatisfactory under certain nonreversal conditions, Fig. 3 indicates good agreement between the predicted and measured dynamic pressures under the reversal conditions ($L_\beta = 0$). Some deterioration in agreement occurs at higher dynamic pressures because of actuator flexibility, which will be discussed later in this section.

Alternatively, the static response may be presented in terms of lift effectiveness L_{eff}, which is the relative measure of loads generated between a flexible and a rigid wing structure. Figures 4–6 show lift effectiveness vs dynamic pressure for three elastic axis configurations, $e/c = -0.08595$, 0, and 0.06365. When $e/c \leq 0$, divergence is not possible; otherwise one must be aware that divergence is present and represents an upper bound on the possible improvement of the reversal conditions. In these figures, a vertical line is placed at λ_{REV} for the TECS-only ($r = 0$) case to serve as a baseline for comparison.

Test velocities are bound due to physical limitations. At low test velocities, frictional forces in the NATA hardware are relatively large in comparison to aerodynamic loads and lead to measurement errors. High test velocities are avoided due to safety concerns for higher-dynamic-pressure tests. As designed with the physical properties of the wing section and NATA parameters in Tables 1 and 2, this system is predicted to become dynamically unstable (i.e., flutter) at approximately $U_{\mathrm{FLUT}} = 12.7$ m/s ($\lambda_{\mathrm{FLUT}} = 1.145$) for $e/c = -0.08595$ and $U_{\mathrm{FLUT}} = 13.4$ m/s ($\lambda_{\mathrm{FLUT}} = 1.275$) for $e/c = 0$. For the $e/c = 0.06365$ configuration, divergence is the limiting case where predictions yield $U_{\mathrm{DIV}} = 18.1$ m/s ($\lambda_{\mathrm{DIV}} = 2.325$). Also, at higher freestream velocities, flow separation at the leading edge becomes a factor (thus a loss of aerodynamic loading occurs), particularly when LECS deflections are large, in addition to higher pitch angles being produced by TECS deflections. The presence of structural damping, including Coulomb friction, increases the onset speed of flutter by approximately 2–3 m/s.

Figure 4 shows predictions and measurements of lift effectiveness for the $e/c = -0.08595$ configuration. Several gearing ratios

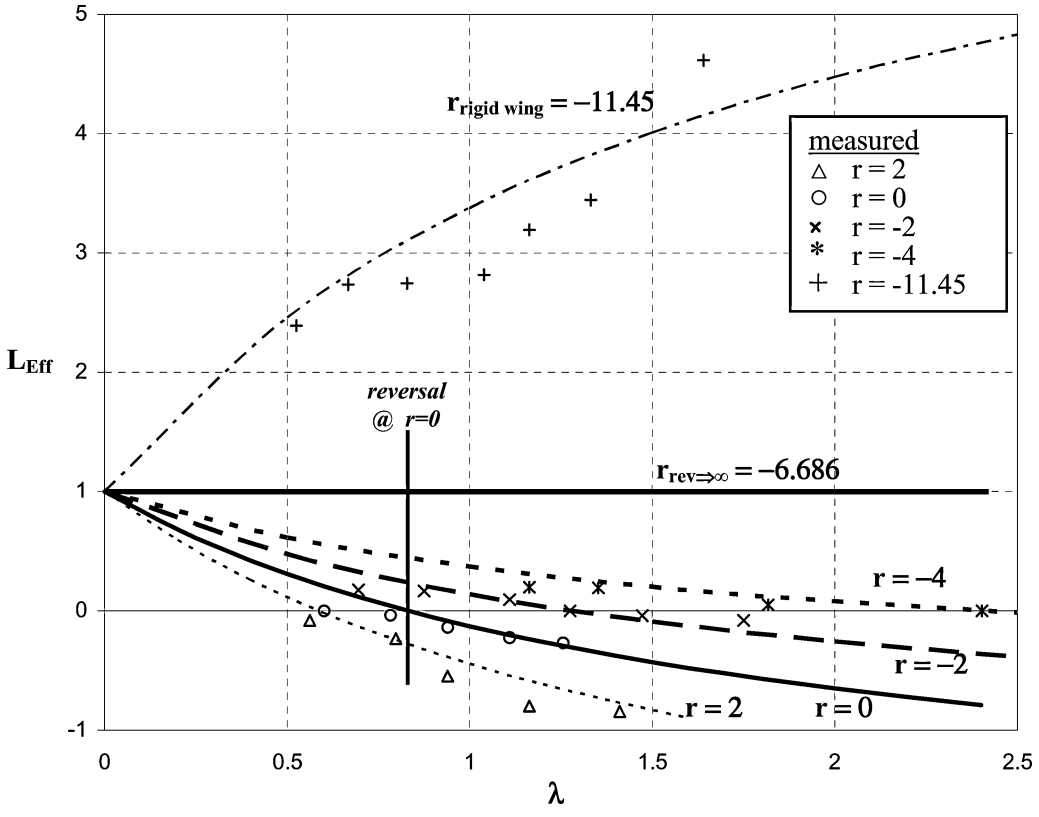

Fig. 4 Lift effectiveness for the $e/c = -0.08595$ configuration. Divergence is not possible.

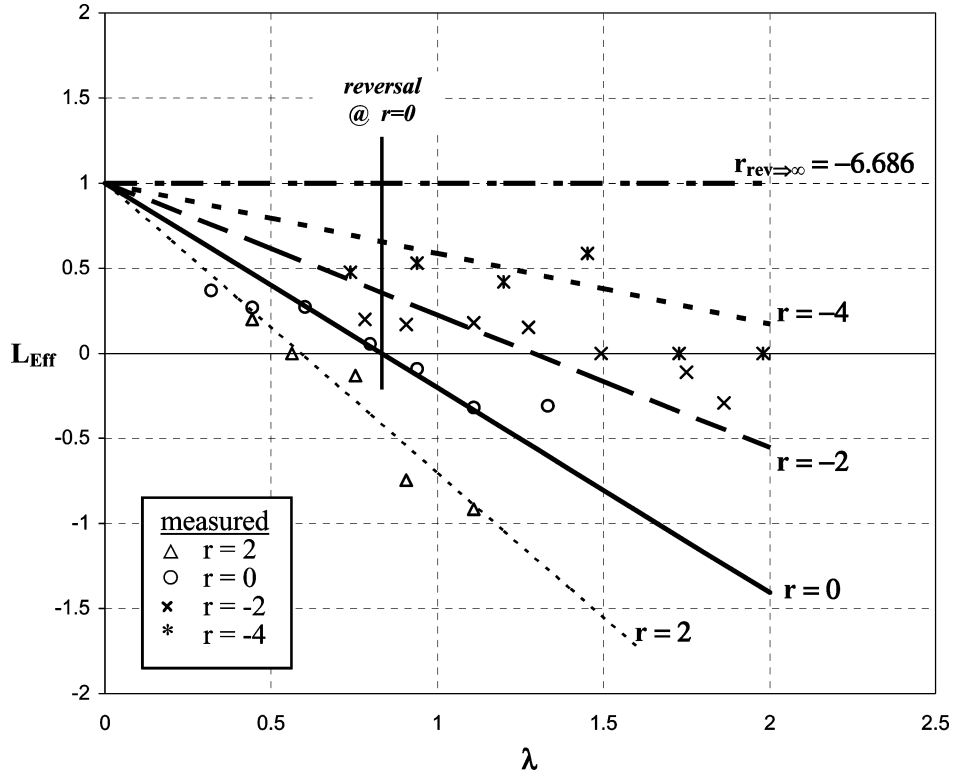

Fig. 5 Lift effectiveness for the $e/c = 0$ configuration. Divergence is not possible.

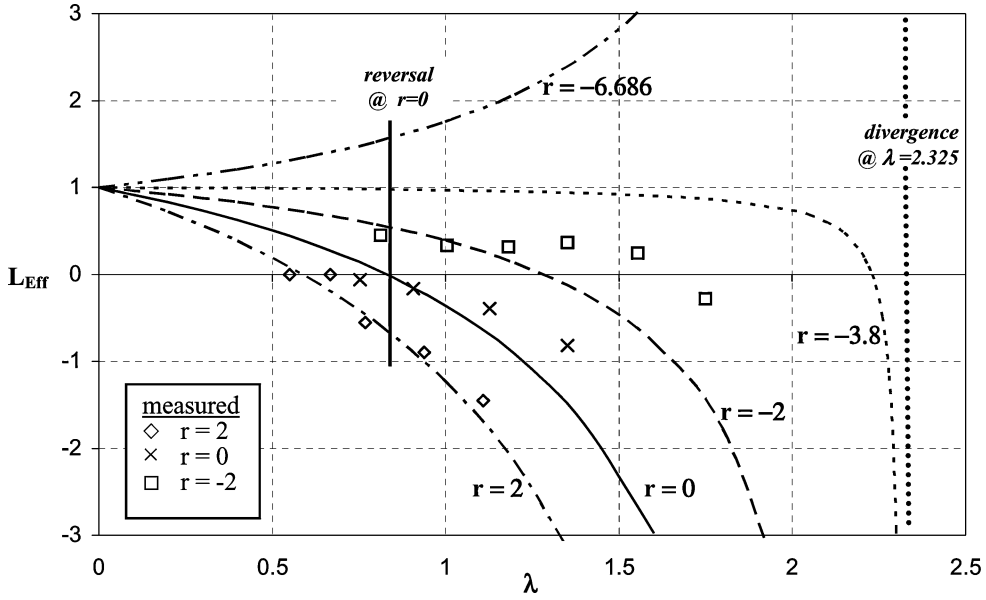

Fig. 6 Lift effectiveness for the $e/c = 0.06365$ configuration. Divergence is possible.

of the control surfaces are examined. This case is identical to that of Fig. 3, except that results use the measure L_{eff} instead of L_β and a few additional gearing ratios are shown. As indicated, reversal is delayed if $r < 0$. For this e/c configuration, $r = r_{q_{\text{REV}} \to \infty} = -6.686$ represents the case in which reversal is completely eliminated and $r = r_{L_{\text{eff}}=1} = -11.45$ represents the rigid wing case. At $r = -6$, reversal is predicted to be nearly eliminated. Although lift effectiveness will eventually become negative, this will occur well beyond the range of the wind tunnel. For $r > 0$, reversal speeds are lowered, suggesting an unfavorable choce.

Figure 5 shows predictions and measurements of lift effectiveness for the $e = 0$ configuration. Note that the same reversal dynamic pressures are predicted as for the prior case of $e/c = -0.08595$. This is expected because reversal is independent of elastic axis position for the typical two-degree-of-freedom section model. Again, the measured data are in agreement with the predicted curves over a limited range of dynamic pressures and deflection ratios. In a manner similar to that shown in Fig. 4, the case for $r = r_{L_{\text{eff}}=1} = -6.686$ (which is also $r_{q_{\text{REV}} \to \infty}$ for the $e = 0$ configuration) is provided, which represents the gearing ratio required to eliminate reversal completely.

Figure 6 shows predictions and measurements of lift effectiveness for the $e/c = 0.06365$ configuration. As a consequence of a positive value of e, Fig. 6 represents a configuration for which divergence is present. For a range of lower dynamic pressures, the experimental data agree with predictions; yet, as dynamic pressure

is increased, flexibility effects, as well as unmodeled flow-separation effects, show a more pronounced difference than the previous results. Simply, the wing section is aeroelastically more sensitive for a system in which divergence is possible. The divergence dynamic pressure is indicated in the figure as a vertical dashed line at $\lambda = 2.325$ ($U = 18.10$ m/s). Reversal occurs below the onset of divergence and, similarly to results in Figs. 4 and 5, reversal is delayed as r becomes more negative. The rigid-wing scenario occurs at $r = r_{L_{\text{eff}}=1} = -3.908$, and a case at $r = -3.8$ is shown to illustrate the response near this case.

One factor that impacts the quality of measured data is actuator flexibility. Extra effort is made to ensure that the desired deflections and gearing ratios of the control surfaces are maintained. Even then, obtaining the precise target gearing ratio is difficult because of actuator flexibility, especially for the LECS, as one might intuitively expect. The static equations developed here assume infinite stiffness for the servomotors. Of interest is the quality of actuator performance as measured by differences between the commanded gearing ratios and those physically affected by unmodeled flexibility, as well as the effect these differences have on measured lift effectiveness. For example, if $r = -2$ is the target, the value obtained after loading may actually be $r = -2.2$. Over the dynamic pressure range of the experiments, when actuator deflections are not readjusted after loading, the true LECS deflection may exceed the commanded deflection by 2–7 deg. For the TECS, the target deflection may exceed the actual deflection by 1–2 deg. Simply, aerodynamic loads affect actuator behavior. Thus, interpretation of the measurements and subsequent comparison with predictions must consider these effects. Alternatively, the analytical model must include actuator flexibility.

Figure 7 compares two sets of experiments with predictions for the $e/c = -0.08595$ configuration. Actuator flexibility is present. In one set of experimental data, the gearing ratio ($r = -2$) is commanded but not confirmed after loading; thus, actuator flexibility is assumed negligible incorrectly. In the other set, the gearing ratio is checked (and adjusted accordingly) after loading. In this case,

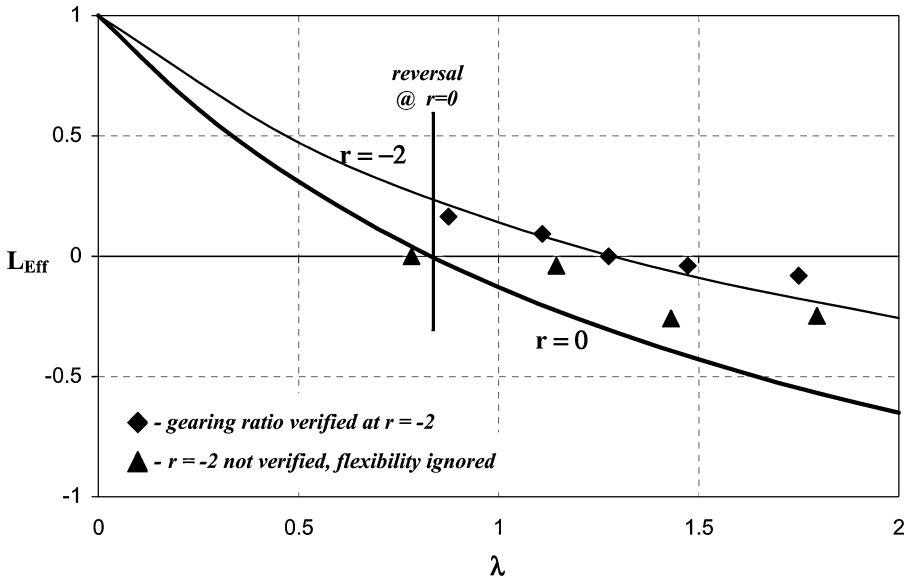

Fig. 7 Actuator flexibility affects lift effectiveness. Experimental and predicted lift effectiveness is compared for the $e/c = -0.08595$ configuration. In one case, actuator flexibility is ignored.

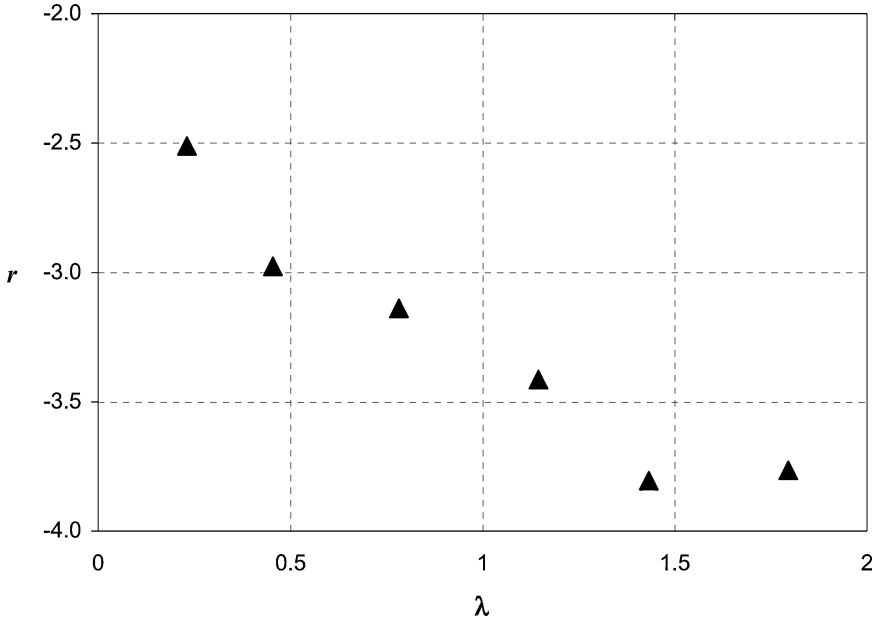

Fig. 8 Actuator flexibility affects the observed gearing ratio. The change of the gearing ratio is shown for increasing dynamic pressure; the commanded value is $r = -2$.

actuator flexibility is considered and the target gearing ratio is achieved. Comparisons with the predicted behavior clearly show that actuator flexibility must be considered. The $r = 0$ (TECS-only) case is presented as a baseline.

Figure 8 shows the gearing ratio without adjustment for flexibility effects for increasing dynamic pressures. Although the gearing ratio is commanded to be $r = -2$, the flexibility of the actuators leads to a change in the observed gearing ratio. Clearly, the effect of flexibility increases with dynamic pressure, and the gearing ratio must be adjusted to achieve the desired setting or analysis must consider the additional control surface rotations accordingly.

Conclusions

The development of the equations for lift effectiveness, reversal, and divergence is presented for the typical two-degree-of-freedom section model with the addition of a leading-edge control surface as well as a conventional trailing-edge control surface. Calculations of static aeroelastic response are made and complementary low-speed wind-tunnel experiments are conducted. Three elastic-axis configurations are examined and include a case in which divergence is possible. By examining the lift effectiveness of the wing section for various deflection ratios (also referred to as gearing ratios) of the leading-edge and trailing-edge surfaces, experiments and calculations demonstrate reversal behavior and validate the concept of using leading-edge control to suppress and possibly eliminate control-surface reversal. Studies examine those cases that produce advantageous lift effectiveness, eliminate control reversal completely, or mimic the performance of a perfectly rigid structure. Also, divergence limitations are examined.

Discrepancies between theory and experiment are attributed to unmodeled flow separation, which mostly affects the contributions from the leading-edge control surface. Also, it is determined that physical restrictions of the experimental hardware limit tests to dynamic pressures sufficiently high to generate quality loading that is unaffected by friction-related forces but low enough to avoid excessive loads and divergence. Finally, the effects of actuator flexibility on the lift effectiveness are examined, demonstrating that experimental and predicted results are impacted adversely by unmodeled actuator flexibility.

References

[1]Dowell, E. H., Crawley, E. F., Curtiss, H. C., Jr., Peters, D. A., Scanlan, R. H., and Sisto, F., *A Modern Course In Aeroelasticity*, 2nd ed., Kluwer, Norwell, MA, 1989, pp. 10–12.

[2]Andersen, G., Kolonay, R., and Eastep, F., "Control Surface Reversal in the Transonic Regime," AIAA Paper 97-1385, April 1997.

[3]Woods-Vedeler, J. A., Pototzky, A. S., and Hoadly, S. T., "Rolling Maneuver Load Alleviation Using Active Controls," *Journal of Aircraft*, Vol. 32, No. 1, 1995, pp. 68–76.

[4]Andersen, G., Forster, E., Kolonay, R., and Eastep, F., "Multiple Control Surface Utilization in Active Aeroelastic Wing Technology," *Journal of Aircraft*, Vol. 34, No. 4, 1997, pp. 552–557.

[5]Dowell, E. H., Bliss, D. B., and Clark, R. L., "Aeroelastic Wing with Leading and Trailing Edge Control Surfaces," *Journal of Aircraft*, Vol. 40, No. 3, 2003, pp. 559–565.

[6]Thompson, David, "Nonlinear Analysis of Store-Induced Limit Cycle Oscillations," M.S. Thesis, Dept. of Aerospace Engineering, Texas A&M Univ., College Station, TX, Aug. 2001.

[7]O'Neil, T. G., "Experimental and Analytical Investigations of an Aeroelastic Structure with Continuous Nonlinear Stiffness," M.S. Thesis, Dept. of Aerospace Engineering, Texas A&M Univ. College Station, TX, May 1996.

[8]Block, J. J., "Active Control of an Aeroelastic Structure," M.S. Thesis, Dept. of Aerospace Engineering, Texas A&M Univ., College Station, TX, May 1996.

[9]Block, J. J., Strganac, T. W., "Applied Active Control for a Nonlinear Aeroelastic Structure," *Journal of Guidance, Control, and Dynamics*, Vol. 21, No. 6, 1998, pp. 838–845.

[10]Strganac, T. W., Ko, J., and Thompson, D. E., "Identification and Control of Limit Cycle Oscillations in Aeroelastic Systems," *Journal of Guidance, Control, and Dynamics*, Vol. 23, No. 6, 2000, pp. 1127–1133.

[11]Strganac, T. W., Ko, J., Thompson, D. E., and Kurdila, A. J., "Investigations of Limit Cycle Oscillations in Aeroelastic Systems," NASA CP-1999-209136, June 1999.

[12]Platanitis, G., and Strganac, T. W., "Control of a Nonlinear Wing Section Using Leading- and Trailing-Edge Surfaces," *Journal of Guidance, Control, and Dynamics*, Vol. 27, No. 1, 2004, pp. 52–58.

[13]Anderson, J. D., Jr., *Fundamentals of Aerodynamics*, 2nd ed., McGraw–Hill, New York, 1991, pp. 282–289.

[14]Bevington, P. R., and Robinson, D. K., *Data Reduction and Error Analysis for the Physical Sciences*, McGraw–Hill, New York, 1992, pp. 96–110.